

Article

Energy Behaviour of Coal Failure under Uniaxial Cyclic Loading/Unloading

Chunlai Wang *, Ze Zhao and Chang Zuo

School of Energy and Mining Engineering, China University of Mining and Technology, Beijing 100083, China
* Correspondence: tswcl@126.com

Abstract: Coal failure is often the precursor of dynamic disaster. The energy evolution behaviour at different stress values was analysed under the gradation of equal amplitude cyclic loading/unloading. Based on the energy dissipation behaviour, the energy evolution model of the coal specimen was established. The multi-parameter energy behaviour predicting model was proposed. Then, the energy storage factor criterion, the energy tangent factor criterion, the energy dissipation growth factor criterion and the energy damage factor criterion of the coal specimen were proposed during the coal fracture process. The energy density and the energy storage status showed different evolution patterns under cyclic loading/unloading. The energy behaviours and status were different in fracture stages of coal specimens, and the dissipated energy behaviour had a sudden response during the failure process. The energy storage and energy dissipation mechanism were related to their respective limits. The energy storage mechanism showed a growth pattern of “low energy promotion, high energy suppression and dissipation promotion, cumulative suppression”. The damage evolution equation and the energy behaviour evolution criterion were established under the cyclic loading/unloading.

Keywords: cyclic loading/unloading; energy behaviour; energy evolution model; predicting criterion



Citation: Wang, C.; Zhao, Z.; Zuo, C. Energy Behaviour of Coal Failure under Uniaxial Cyclic Loading/Unloading. *Appl. Sci.* **2023**, *13*, 4324. <https://doi.org/10.3390/app13074324>

Academic Editor: Arcady Dyskin

Received: 27 February 2023

Revised: 23 March 2023

Accepted: 24 March 2023

Published: 29 March 2023



Copyright: © 2023 by the authors. Licensee MDPI, Basel, Switzerland. This article is an open access article distributed under the terms and conditions of the Creative Commons Attribution (CC BY) license (<https://creativecommons.org/licenses/by/4.0/>).

1. Introduction

Coal material is a complex natural geological medium that contains many randomly distributed flaws, such as natural joints and cracks [1–4]. Coal fracture is a mechanical behaviour of status instability under the action of energy [5–7]. Many well-established theories for the observation, identification and analysis of microcracks in rock and coal samples have been proposed [8–11]. Coal material often shows different mechanical characteristics that are associated with the cycle number under loading/unloading [12–15]. Therefore, energy behaviour was considered essential to describe the energy state and stability of coal materials. Rocks fracture during axial compression to absorb energy, and they fracture under closed pressure reduction to release energy. Energy evolution models and energy evolution behaviour are recognized as the basis for design and evaluation in rock engineering, and it is one of the key problems in underground engineering [16–18].

The main purpose of this study is to develop an understanding of damage and deformation characteristics under cyclic loading/unloading. Many researchers have made contributions to the study of the strength and deformability of rocks and coal materials under cyclic loading conditions. In these studies, the damage variable was described for the rock failure behaviour under cyclic loading, as the closure pressure increases, the axial strain at damage increases, as does the residual volume strain at the beginning of expansion [19,20]. Based on this, the energy evolution mechanism and the evaluation model of dissipated energy were proposed based on the energy principle of rock damage. This was a meaningful finding for rock damage by studying the energy storage and dissipation characteristics of rocks at different deformation stages, and using the energy principle of damage to derive the energy intensity criterion [21–23]. Meanwhile, the fatigue evolution of rock materials was crucial to the stability of engineering structures under cyclic loading, for

a given energy condition, rocks yield more easily at low frequencies and amplitudes than at high frequencies and amplitudes [24,25]. Therefore, many researchers have investigated the damage of rock materials under cyclic loading. For example, the damage evolution pattern of rocks was analysed in multi-valued amplitude cyclic loading tests at different confining pressures [26–28]. After this, the energy dissipation characteristics of coal specimens were used to describe the propagation of crack growth behaviour under layered cyclic loading [29,30]. In particular, the peak stress of cyclic loading has a strong influence on the fatigue behaviour of coal specimens and the degree of damage increases with increasing energy dissipation density [31,32].

Up to now, it has been shown that the damage pattern of specimens under cyclic loading is different from the damage pattern under static loading, and some studies have also advanced the constitutive relations and damage behaviour aspects of rocks under quasi-dynamic loading. However, the dynamic damage of rocks from an energy perspective remains unclear, especially in cyclic loading condition. The results of the exploration of the relationship between energy transformation and coal damage showed that the energy behaviour was different at different stages of deformation [33–36]. Therefore, the energy density of rock materials increased nonlinearly under different loading/unloading rates; it is also worth noting that the loading and unloading speed has a considerable effect on the dissipated energy density [37–39]. In actual projects, rock materials are usually loaded/unloaded repeatedly, such as in coal mining, tunnel excavation and roadway support [40]. The strength and deformability are closely related to the stress state and loading history. It was widely accepted that the damage evolution was driven by energy, and different stress paths had different mechanical behaviour and energy conversion characteristics. This is also a feasible way to reveal the phenomenon of energy release and stress dissipation during rock destruction from the perspective of energy [41–44]. The damage variable of the coal materials was defined by different parameters under cyclic loading/unloading, but the description of other mechanical behaviours of rock samples was ignored. Moreover, it was not comprehensive to describe the failure characteristics of rocks only using the damage variable, which is defined by dissipative energy. It also ignored the influence of other energy behaviours on their failure state under the cyclic loading/unloading process. Therefore, the energy behaviour and evolution patterns of coal specimens under different stress paths were explored, and the prediction model of energy evolution of coal specimens was also constructed. In view of this, this paper provided a theoretical basis for the stability analysis of engineering structures, and has practical engineering application value.

2. Experiments and Methods

2.1. Specimen

The coal sample collection area is a monoclinic structure with the overall direction of north-east, inclination of north-west and dip angle of about 3° . No fault or obvious fold structure are found in the mining area, and there are no magmatic rocks, only some wide and gentle undulations are developed above the framework of the monoclinic structure. The thickness of the seam in the mining area was 142.09~267.46 m, with an average of 169.29 m. The value of true density was between 1.38 and 1.52, and the value of apparent density was between 1.28 and 1.39. The specimens were selected from the same value for processing, sampling and testing. The coal sample was processed into a cylindrical piece with the size of 50 mm × 100 mm. The coal specimens were carefully ground to ensure that the two ends were smoothed without major damage. The non-parallelism of the coal specimen should not exceed 0.05 mm, and the deviation should not be more than 0.25° in the axial direction. In this study, a total of 10 standard coal specimens were processed as shown in Figure 1.



Figure 1. Partial test coal specimens after processing.

2.2. Experimental Equipment

The loading equipment was a Yaxing YDSZ-2000 (Yaxing Numerical Control Technology Co. Ltd., Changsha, China) which was controlled by microcomputer, as shown in Figure 2. The acoustic emission (AE) monitoring equipment was a PCI-II AE signal acquisition and analysis system (Physical Acoustics Corporation, Princeton, NJ, USA). AE signals could be acquired, displayed and stored during the whole loading process. To ensure and improve the spatial positioning accuracy of the AE events during the loading process, the arrangement of the AE sensors was as follows: they were placed 20 mm away from the end of the coal specimen and it should be ensured that the AE sensors were at an angle of 90° to each other, and all AE sensors should not be coplanar. According to the noise value of the laboratory, the threshold of the AE system was set to 45 dB, the sampling rate was 1 MHz, the gain of the preamplifier was set to 40 dB and the data were collected by 6 channels in this experiment. The layout of the AE monitoring equipment is shown in Figure 2.



Figure 2. Mechanical loading equipment and AE system.

2.3. Experimental Process

The stress–strain curve of the coal specimen could well describe the basic mechanical behaviour of coal under the uniaxial loading. The coal strength under the uniaxial static loading could be used as a reference to estimate the strength under uniaxial cyclic loading/unloading. Then, the upper and lower limit stress value would be determined by the strength under uniaxial static loading.

To reduce the influence of the friction noise of the press head and the end of the specimen on the AE signal, an appropriate amount of Vaseline was applied between the sensor and the surface of the coal specimen. The AE sensors were fixed by tape at both ends of the specimen and the press head, and the loading/unloading rate was controlled at 0.05 MPa/s. It should be ensured that the AE monitoring and loading process was always synchronized. Therefore, the AE monitoring system and the loading device should be proofread and unified before the test. The loading system recorded the deformation and strength parameters of the coal specimen, and the AE monitoring system monitored the deformation and damage process of the coal specimen.

With respect to the type of the cyclic loading/unloading, it was mainly divided into two kinds of stress paths. The first method was the grading cyclic loading/unloading and the repeated cycles' influence on fracture behaviour was analysed by this method. Moreover, the mechanical response characteristics and energy distribution state of the coal specimens were also investigated under different stress gradients. The second method was the equal amplitude cyclic loading/unloading. It was mainly used to explore the influence of continuous cyclic loading/unloading on the damage state under different stress values. Meanwhile, it was also used to analyse the effects of different cyclic times on the fatigue damage state under the same stress value.

3. Theoretical Basis

3.1. Energy Conversion of the Coal Specimen

Under the action of energy drive, the macroscopic fracture and deformation of the coal specimen occurred, and the input energy was stored or dissipated in different forms, as shown in Figure 3. Part of the energy would be stored in the form of elastic strain energy U_e . Some energy U_d would be dissipated during crack initiation, propagation and plastic deformation. In addition, a small amount of energy U_r would be dissipated in different ways, such as thermal radiation, thermal conduction and ejection kinetic energy [45–47]. Since this part of energy took up a relatively small proportion and had a small impact on the failure state and failure stage of coal specimens, it was ignored and will not be discussed in this paper.

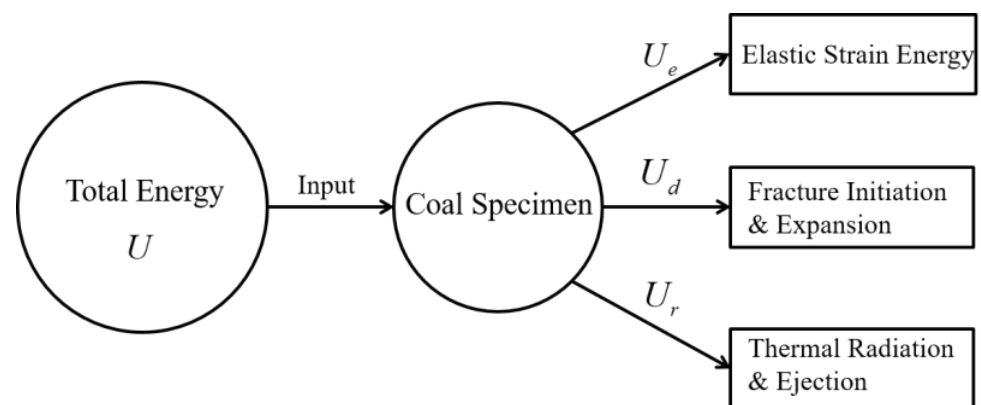


Figure 3. The energy conversion of coal specimen in the failure process.

3.2. Energy Calculation of the Coal Specimen

Under the action of axial loading, the coal specimen produced strain and accumulated energy. Equation (1) is the energy integral formula [48]. Since the radial strain value of coal specimen was low, the energy generated by radial strain was not considered in this paper.

$$U = \int \sigma d\varepsilon = \sum_{i=0}^n \frac{1}{2} (\varepsilon^{i+1} - \varepsilon^i) (\sigma^i + \sigma^{i+1}) \quad (1)$$

where the U is the total energy absorbed under the action of axial force, the σ^i is the axial stress and the ε^i is the axial strain.

In fact, the total energy can be converted into two parts, one is the elastic strain energy U_e stored in the coal specimen, and the other is the dissipated energy U_d consumed by the coal specimen. Under the action of axial loading, the stored elastic strain energy at a certain t moment can be expressed as Equation (2) [49]:

$$U_e = U - U_d = \frac{1}{2E_i}\sigma^2 \quad (2)$$

As shown in Figure 4, the loading process is represented by a solid line and the unloading process is represented by a dotted line. The area between the loading curve (OA) and the transverse axis of the first cycle is the total strain energy generated by the coal specimen under external loading. The area between the unloading curve (AEBC) and the horizontal axis of the first cycle is the elastic strain energy released by the coal specimen. The plastic strain energy is equal to the area under the loading curve, and the difference between the area under the unloading curve and the area of the hysteresis loop, which is the dissipated energy required to produce a new crack.

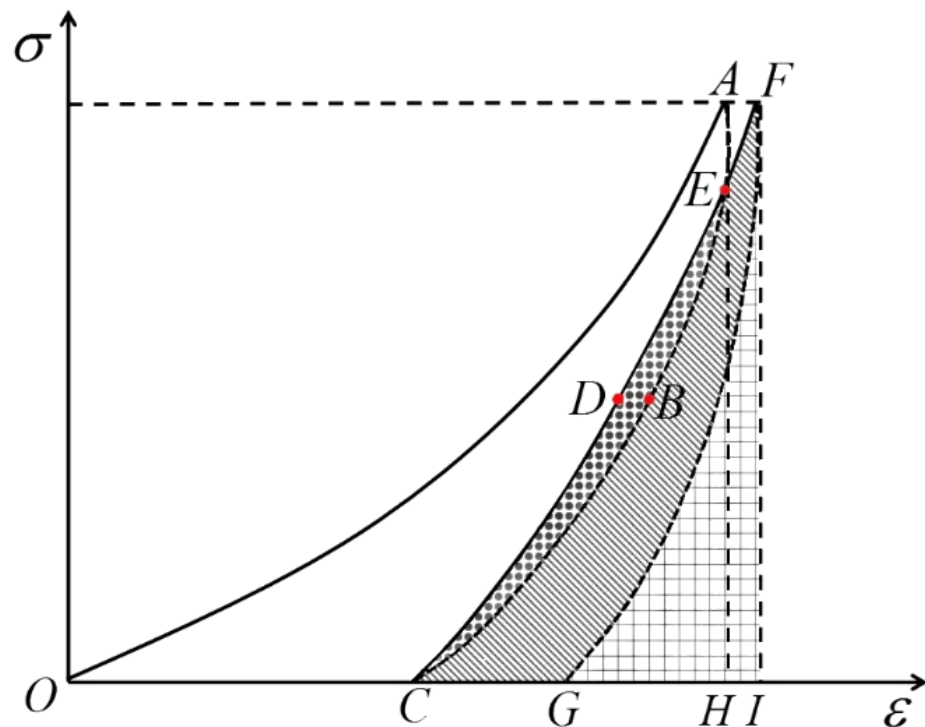


Figure 4. The elastic and plastic strain energy calculation under loading/unloading. The red dots indicate the critical points of dissipated energy required to create new cracks.

4. Results and Analysis

4.1. The Characteristics of AE Energy under Cyclic Loading/Unloading

4.1.1. AE Energy under Gradation Cyclic Loading/Unloading

During the grading cyclic loading/unloading process, the AE energy count of the coal specimen shows a sudden increased effect in the peak stress of each graded stage, as shown in Figure 5. As AE energy count can reflect the intensity and frequency of AE signals, it can be seen that AE signals will be generated with higher intensity than in the previous loading stage when each stress loading stage reaches a new stress peak. However, the AE energy count at the peak of 0–4 MPa is slightly higher than the peak stress of the 2–6 MPa stage.

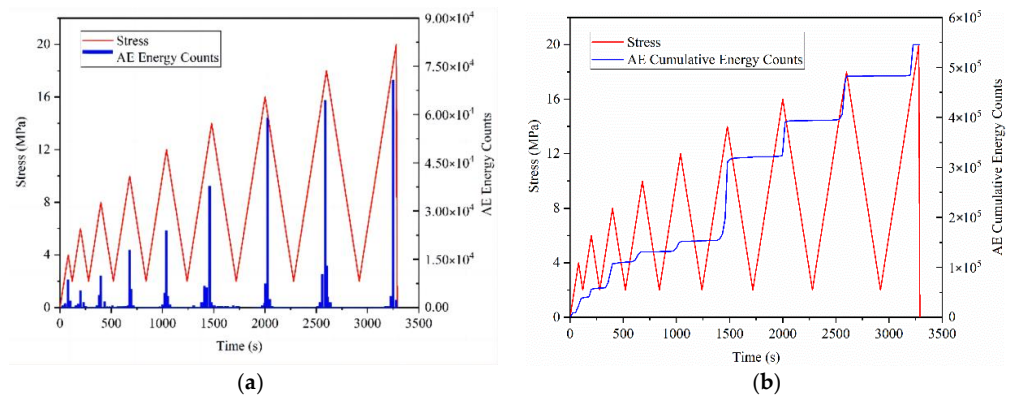


Figure 5. The AE energy characteristics of AC1 coal specimen; (a) Stress–Time–AE energy counting curve; (b) Stress–Time–AE cumulative energy counting curve.

The AE energy count shows the evolution trend of a small decline (compacting stage)–stable large rise (linear elastic phase)–slow rise (plastic deformation phase)–disappearance (fracture instability phase). The cumulative AE energy count presents an obvious step-like curve feature. When each graded stress reached the peak, the accumulated AE energy counts show a good “stepped” rise characteristic. The accumulated AE energy counts change a little during the unloading phase, they continue to change with a small increase or retention. It also can be observed that each higher stress than the previous stage will cause a large number of new AE events, especially at the peak stress. The cumulative AE energy counts also show the characteristic of an extreme speed increase in the new stress phase.

4.1.2. AE Energy under Equal Amplitude Cyclic Loading/Unloading

It can be known that the failure strength of the coal specimen is reduced when compared with the staged cyclic loading/unloading, and the failure strength is approximately 16 MPa, as shown in Figure 6. The process of the equal amplitude under cyclic loading/unloading is mainly divided into three stages: 0–5 MPa (the compaction stage), 5–10 MPa (the linear elastic deformation stage) and 10–15 MPa (the plastic deformation stage). This is mainly used to analyse the damage degree of the coal specimen at different deformation stages. It can be seen that when the stress reaches the peak stress for the first time in each stress stage, AE energy counts shows a sudden increase, and there is a significant decrease in the subsequent cycle stage compared with the first time. The cumulative energy counts of AE shows simultaneously an obvious “step-like” growth characteristic and the sudden increase at the stress peak. The sudden increase effects at the first stage (0–5 MPa) are much smaller than that at the second stage (5–10 MPa) and the third stage (10–15 MPa). This indicates that the AE activity at the compaction stage is much smaller than that at the stage of elastic deformation and plastic deformation.

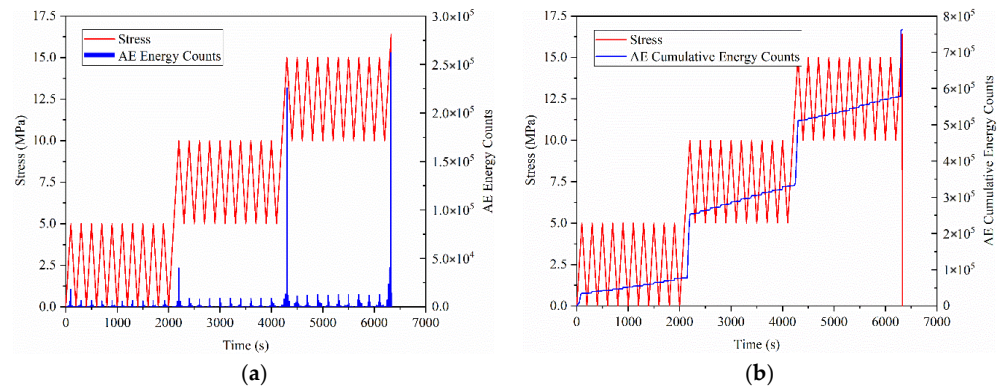


Figure 6. The AE energy characteristics of BC1 coal specimen; (a) Stress–Time–AE energy counting curve; (b) Stress–time–AE cumulative energy counting curve.

4.2. Energy Evolution Characteristics of the Coal Specimen

4.2.1. Evolution Characteristics of Energy Storage Rate

The Evolution Characteristics of the Energy Storage Rate under Grading Cyclic Loading/Unloading

The elastic energy storage rate and the dissipative energy dissipation rate are important indicators which can demonstrate the energy storage state of the coal specimen. It is also an important indicator in engineering practice. The definition and calculation formula of the storage rate and the dissipation rate can be expressed as:

$$k_{SF_e} = \frac{U_e}{U} \tag{3}$$

$$k_{SF_d} = \frac{U_d}{U} \tag{4}$$

where the k_{SF_e} is the storage rate of the elastic energy the k_{SF_d} is the dissipation rate of dissipated energy; the U_e is the elastic energy, J/mm^3 ; the U_d is the dissipated energy, J/mm^3 and the U is the total energy accumulation of the coal specimen, J/mm^3 .

It can be known that the elastic energy storage rate of the coal specimen is at lower values at stage I, but the rising rate value rises rapidly and faster from 0.2 to 0.8, as shown in Figure 7. It maintains steady development trend at stage II. The elastic energy accounts for slightly downward values, but they have remained at a higher value (around 0.84) at stage IV. Conversely, the dissipative energy dissipation rate shows an extremely rapid downward stage I. At stage II, it remains at a low value of about 0.12. At stage IV, the proportion of dissipated energy has a slight upward trend, but it still remains at a low value of 0.16. The elastic energy is lower at stage I, and the dissipation energy is higher. The main reason was that the input of total energy was less and the elastic deformation occurred less, so most of the energy was mainly used for the original and irreversible fracture and deformation, and more energy was wasted at this stage. Both the dissipated energy and the elastic energy basically maintained a stable value state at stage II. As the coal specimen entered the yield deformation stage, a large amount of plastic deformation occurred inside the coal specimen. Therefore, the proportion of the dissipated energy will increase to a certain extent.

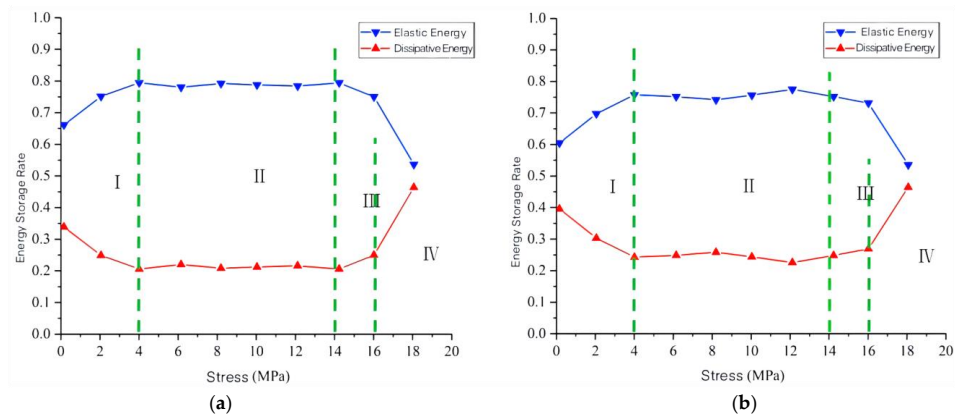


Figure 7. The energy storage rate evolution under staged cyclic loading/unloading. The green line is used to delineate the different stages through which the coal samples in the diagram have gone. (a) Variation curves of elastic energy storage rate and energy dissipation rate of coal sample S1. (b) Variation curves of elastic energy storage rate and energy dissipation rate of coal sample S2.

The Evolution Pattern of the Energy Storage Rate during the Equal Amplitude Loading/Unloading

The proportion of dissipated energy of coal specimens is much larger in the first cycle than that in the follow-up cycle stage, as shown in Figure 8. In the first stage (0-5-0 MPa), the dissipated energy storage rate is basically in a stable state of fluctuation, and does

not change significantly. However, the dissipative energy dissipation rate is high. In the second cycle stage (5-10-5 MPa), the changes of energy storage rate and dissipation rate are relatively stable, and the elastic energy storage rate is always maintained at a high value. The third stage (10-15-10 MPa) mainly took place after the yield stage, and a large amount of plastic deformation occurred in this stage and it is not recoverable. Then, the energy dissipation rate increases to a higher value, while the storage rate of elastic energy decreases to an appropriate degree.

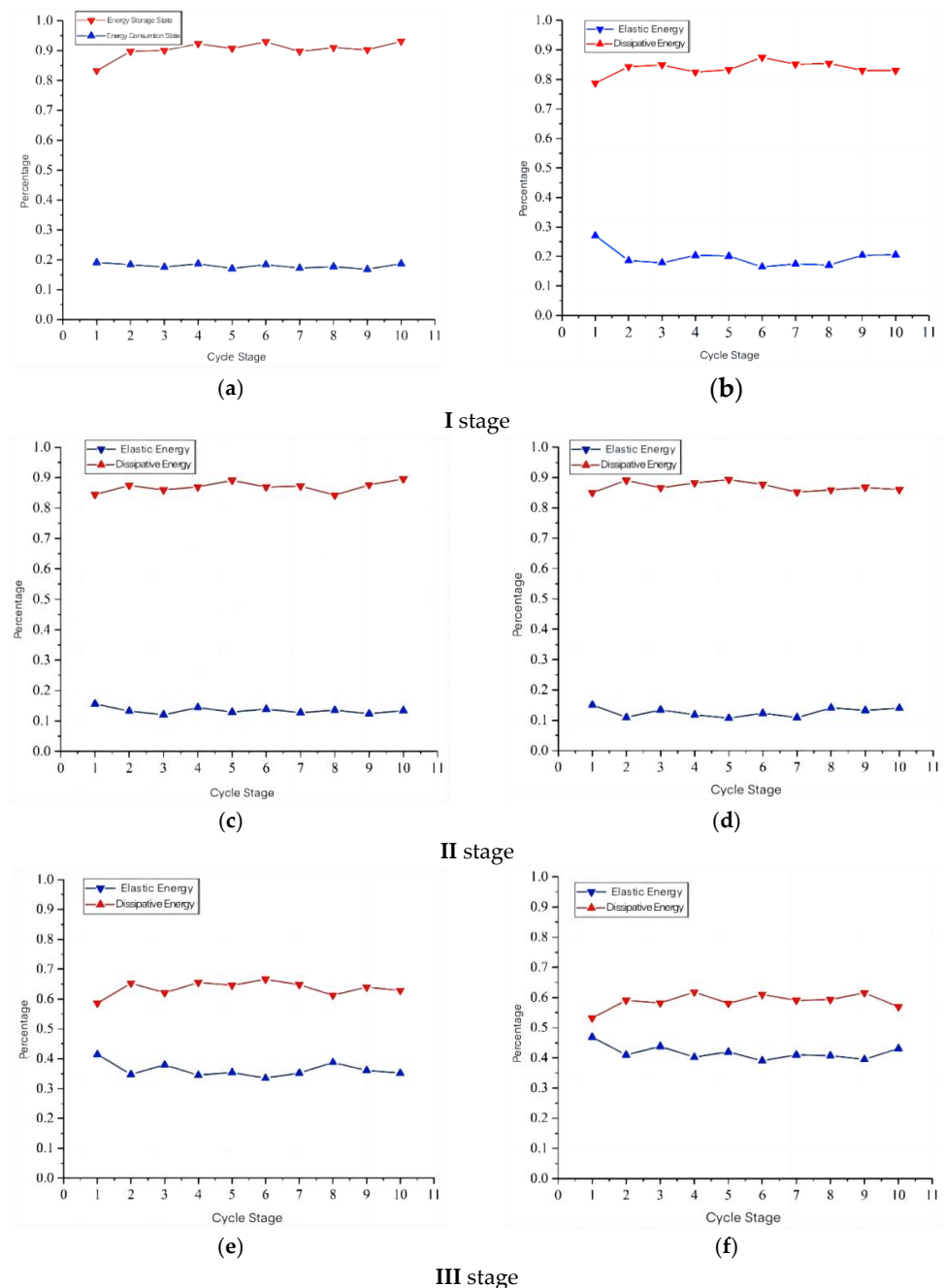


Figure 8. The energy accumulation and dissipation during equal amplitude loading/unloading. (a) Results of cyclic loading of coal sample S3 in stage I (b) Results of cyclic loading of coal sample S4 in stage I (c) Results of cyclic loading of coal sample S3 in stage II. (d) Results of cyclic loading of coal sample S4 in stage II. (e) Results of cyclic loading of coal sample S3 in stage III. (f) Results of cyclic loading of coal sample S4 in stage III.

The pattern of the energy evolution can reflect the energy storage state and energy consumption state as well as the stability degree and damage situations. It shows a higher elastic energy storage rate and lower energy dissipation at low stresses. The reason for this was that the coal specimen mainly showed the closure of the original crack and produced new cracks at the low stress. Moreover, the damage degree of the coal specimen was relatively low or basically did not occur. Therefore, the elastic energy storage rate of the coal specimen was relatively large. In the second stage, the coal specimen underwent the linear elastic reversible deformation, so the elastic energy was greatly improved. In the third stage, the coal specimen produced unrecoverable plastic deformation, thus, the dissipation rate could provide a larger value. It also indicated that the coal specimen can produce a large amount of fracture behaviour at this stage. The energy status was close to the limitation of energy storage and energy consumption. Furthermore, the coal specimen was in critical stable state.

4.2.2. Evolution Characteristics of Energy Tangent Factor

The change rate of the energy is a very important parameter for judging the state of the coal specimen. It is also of great significance for judging the energy evolution stage and energy drive mechanism. To show the change of energy growth rate of the coal specimen under axial load, the energy growth tangent factor was proposed. The calculation formula can be expressed as Equation (5):

$$k_{TF} = \frac{dE_i}{d\sigma_i} = \frac{\Delta E}{\Delta\sigma} \tag{5}$$

where the k_{TF} represents the energy tangent factor; the energy factor increment $\Delta E = E_{i+1} - E_i$, and the stress increment $\Delta\sigma = \sigma_{i+1} - \sigma_i$.

Energy Growth Pattern under Graded Cyclic Load

It can be known that the elastic energy growth rate keeps increasing, while the dissipative energy tangent factor fluctuates at a low value at stage I, as shown in Figure 9. It mainly shows crack closure and cracking behaviour in this stage, and there is basically no plastic deformation. Therefore, the elastic energy tangent factor is continuously increasing. The tangent factor of elastic energy fluctuates at a higher value, and the dissipative energy tangent factor also fluctuates after a certain jump at stage II. The reason for the jump of the dissipative energy tangent factor was that the deformation gradually reached the yield stage with the increase of crack growth, and irreversible plastic deformation occurred in the coal specimen. Then, it would lead to a step-like jump of dissipative energy tangent factor.

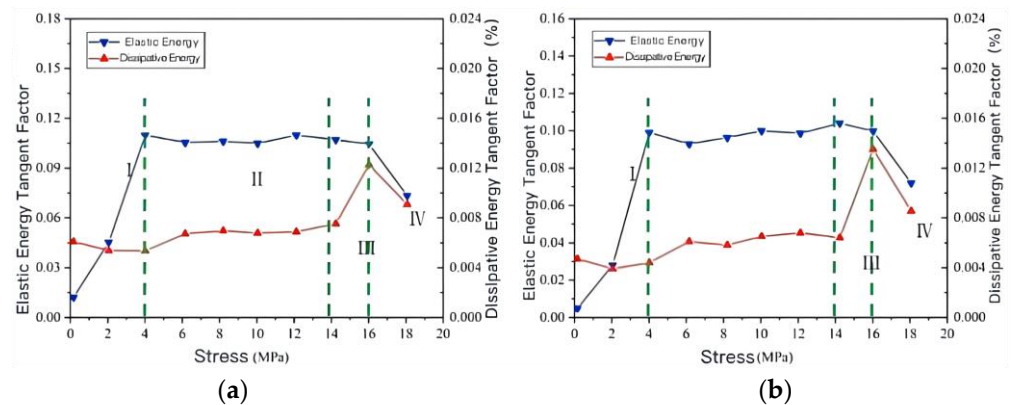


Figure 9. The energy tangent factor during grading cyclic loading/unloading. (a) Elastic energy tangent factor and dissipative energy tangent factor of coal sample S1. (b) Elastic energy tangent factor and dissipative energy tangent factor of coal sample S2.

It can be known that the tangent factor curve of elastic energy and dissipative energy shows a large value of continuous decline at stages III and IV. This was mainly caused by how the high energy storage state inhibited the energy storage capacity of the coal specimen. When the coal specimen is in a high energy state, the stable state decreases, and the energy storage rate decreases after being restrained. Therefore, the variation of the energy tangent factor exists in the state of “promoting storage with low energy and inhibiting storage with high energy” under different stress states.

Energy Growth Pattern under Equal Amplitude Cyclic Load

It can be known that the tangent factor of elastic energy and dissipative energy are both in stable fluctuation during the equal amplitude loading/unloading. The change of the energy growth rate will only fluctuate to a certain extent, as shown in Figure 10. However, the energy tangent coefficients are different for different deformation or stress states. The elastic energy is at a lower value in the first stage and at a higher value in the second stage. Furthermore, it is also at a lower value in the third stage, but still higher than the first stage. The change of dissipative energy tangent factor also shows a change trend of low value rise–high value maintain–second high value decline. It indicates that there also exists a “low facilitation, high inhibition” model of change.

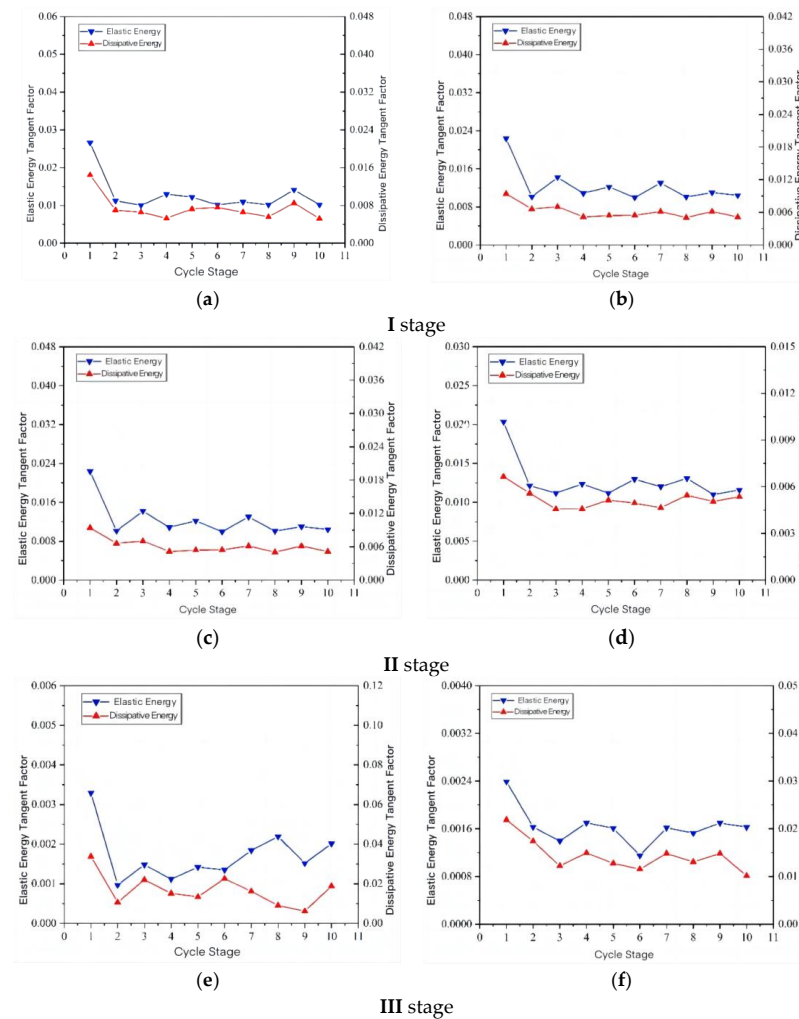


Figure 10. The energy tangent factor under equal amplitude cyclic loading/unloading. (a) Elastic energy tangent factor and dissipative energy tangent factor of coal sample S3 in stage I. (b) Result of coal sample S4 in stage I. (c) Result of coal sample S3 in stage II. (d) Result of coal sample S4 in stage II. (e) Result of coal sample S3 in stage III. (f) Result of coal sample S4 in stage III.

4.2.3. Evolution Characteristics of Energy Damage Factor

Different energy states are likely to induce different energy behaviours to characterize the damage degree of the coal specimen. In particular, the dissipated energy state can be used to describe the deformation and stability degree of the coal specimen to some extent. Therefore, the energy damage variable was proposed by the dissipation energy. It can be expressed as Equation (6):

$$k_{DF} = \frac{U_{d_n} - U_{d_m}}{U_{max} - U_{d_0}} \tag{6}$$

where the k_{DF} is the damage variable of the coal specimen; the U_{d_n} is the dissipated energy state under the stress value, n ; the U_{d_m} is the dissipated energy state under the stress value, m , and $n > m$; the U_{max} is the dissipated energy under the highest stress value of coal specimen and the U_{d_0} is the dissipated energy state at the initial stress stage.

It can be known that the damage state of the coal specimen is quite different at different stress stages, as shown in Figure 11. When $\sigma/\sigma_p \leq 0.1$, the damage status is at a low level. However, with the increment in stress, the damage variable shows fast growth. This was mainly related to the rock cracks' initiations. The energy state was continuously improved. After the accumulated energy broke the minimum activation energy of rock cracks, these cracks began to expand. At the moment of rock crack initiation, it had a great influence on the damage state of the coal specimen. In a short time, the damage variable increased to a large extent. When the stress continued to increase, it entered a stable elastic deformation stage. When the stress (σ/σ_p) was within the range of 0.2~0.75, the dissipated energy did not increase significantly. In fact, the energy damage variable also changed gently and gradually increased at a nearly gentle rate. It meant that the damage state had not changed significantly, and the crack growth was gentle and stable. The damage state showed a high mutation when the stress σ/σ_p was greater than 0.85. This indicated that the dissipated energy played a leading role in this stress level. Then, it could cause greater damage over a small stress gradient, and the damage variable reached the peak state before the critical peak stress.

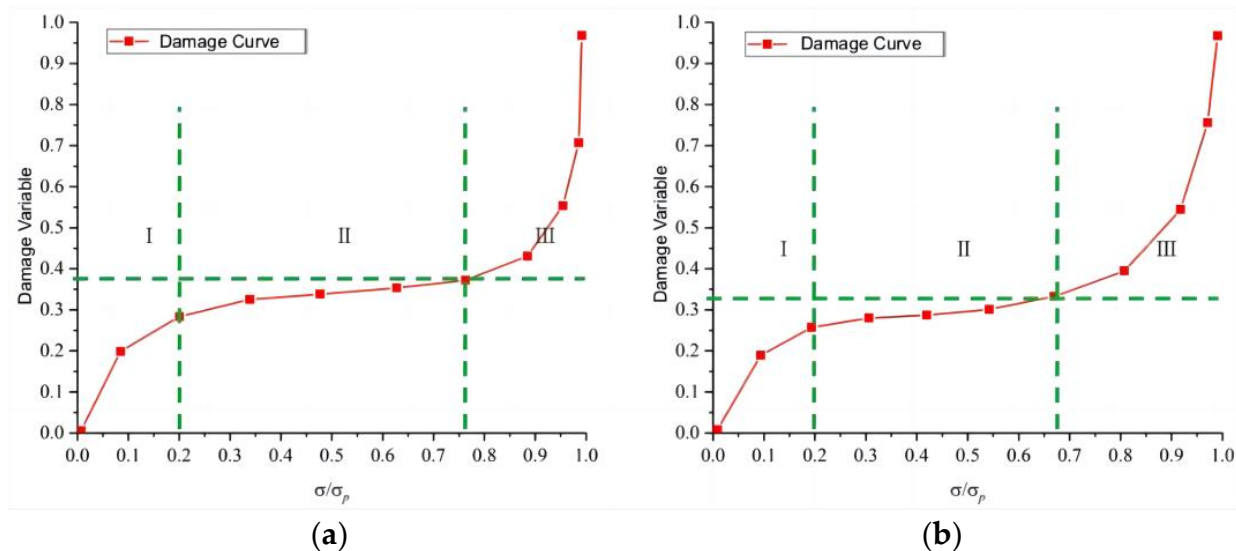


Figure 11. The damage variable evolution of the coal specimen in the fracture process. The green line is used to delineate the different stages through which the coal samples in the diagram have gone. (a) The damage variable evolution of the coal sample S1. (b) The damage variable evolution of the coal sample S2.

The damage variable showed the characteristics of the phases during the cyclic loading. In the elastic deformation stage, the damage variable increased slightly and slowly. In the critical fracture stage, the energy damage variable showed a high mutation, which

indicated that the coal specimen was completely destroyed. Therefore, the energy damage variable displays a pattern of the small rapid growth–slow growth–jump mutation state.

4.3. Energy Evolution Model of Coal Failure Process

The coal specimen was loaded with cyclic loading/unloading at the same stress value, which would have a significant impact on its damage and deformation, and it would further affect the energy state and stability. The damage was closely related to the number of cycles. For the cyclic loading/unloading, if the number of cycles was 0 ($N = 0$), the coal specimen was intact ($D = 0$). When the cycle numbers reached the maximum cycle number ($N = N_f$), the damage of coal specimen is more serious. Then, the damage variable reached the peak value, and it may be a failure. The relationship between the damage variation and the cycle numbers can be expressed as Equation (7):

$$D = 1 - [1 - (\frac{N}{N_f})^{\frac{\beta}{1-\alpha}}] \tag{7}$$

where the D is the damage variable of coal specimen; the N is the cycle numbers of coal specimen under the same stress value; β is the stress-related constant of the loading process of the coal sample, the larger β the greater the damage to the coal sample during the destruction process and the α is the stress index of coal specimen, which can be expressed as Equation (8):

$$\alpha = 1 - \gamma(\frac{\sigma_{max} - \sigma_f}{\sigma - \sigma_{max}}) \tag{8}$$

where the γ is the coefficient related to the properties of coal specimen and it is a constant; the σ_{max} is the maximum axial stress; the σ_f is the threshold of yield stress and the σ is the stress value under any strain state of the coal specimen.

The dissipated energy evolution curve of the coal specimen is shown in Figure 12. The dissipated energy state evolution equation is as below during the failure process. It is shown that the Equation (9) can well coincide with the evolution pattern of the energy state under axial cyclic loading.

$$U_d = (1 - \nu)E_0 \frac{1}{1 + e^{-(\epsilon - \epsilon_c)^2 + \zeta}} \tag{9}$$

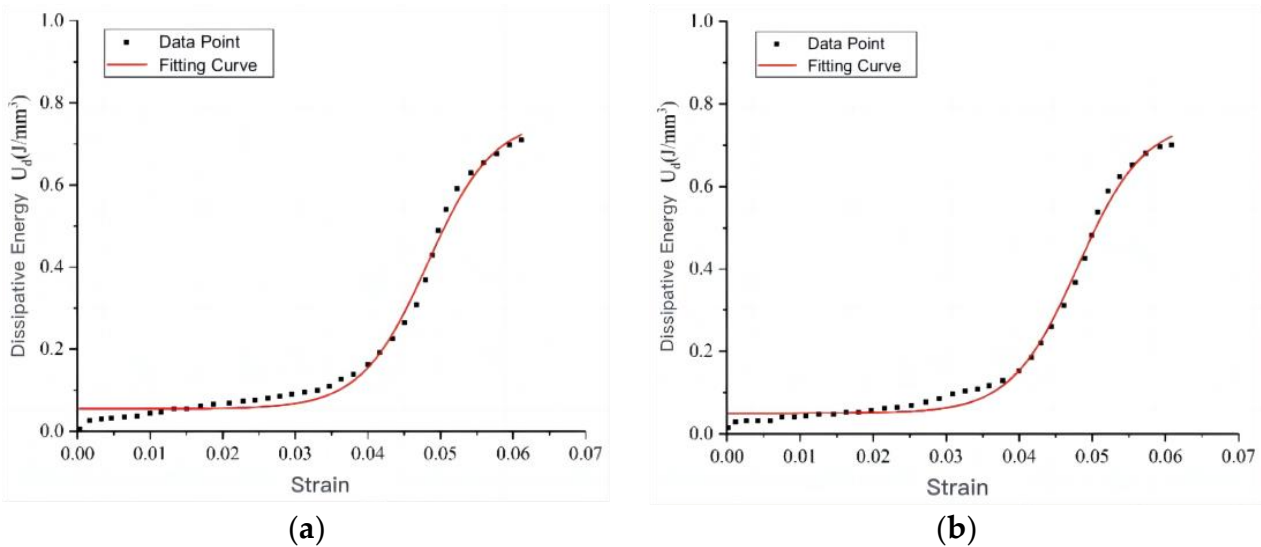


Figure 12. Trend diagram of coal specimen dissipation energy under axial cyclic loading. (a) The dissipated energy evolution curve of the coal sample S1. (b) The dissipated energy evolution curve of the coal sample S2.

The dissipated energy behaviour of the coal specimen had obvious evolution characteristics under axial cyclic loading. The dissipative energy behaviour of coal specimens has a distinct evolutionary feature under axial cyclic loading. Therefore, the energy state evolution equation can represent the energy state evolution mode of coal specimens. An energy evolution model was used to describe the energy state and stability of the coal specimen.

The cumulative micro-flaws can represent the failure state and stability degree of the coal specimen to a large extent. The calculation formula for the generation of micro-flaws is Equation (10).

$$V(\varepsilon) = A \frac{\alpha}{\gamma} e^{(-\frac{U_0}{\alpha})} [e^{(\frac{\gamma \varepsilon U_d(\varepsilon)}{\alpha})} - 1] \tag{10}$$

where the v_ε is the formation rate of the micro-crack in the coal specimen which related to strain parameters; the A , γ and α are parameters that related to the properties of coal specimens and they are constant; The U_0 is the minimum activation energy generated by micro-flaws in the coal specimen and the $U_d(\varepsilon)$ is the energy state of the dissipated energy.

The coal failure is closely related to its energy state and strain characteristics. Therefore, when the coal failure stress (σ_c) reaches the peak value, the relationship between the coal's strength (σ_c) and the energy state is Equation (11).

$$\sigma_c = \frac{1}{\gamma} [\alpha \ln(\frac{\gamma \varepsilon}{\alpha} U_d(\varepsilon) + e^{-\frac{U_0}{\alpha}}) + U_0] \tag{11}$$

This equation expresses an energy destruction criterion for coal fracture evolution characterized by the dissipation energy. In fact, when the coal specimen reached the threshold of yield stress σ_f under the axial loading, it had already entered the critical failure state.

Therefore, the point of the dissipated energy state $U_{fd}(\varepsilon)$ could be taken as the key predicting point of the failure of the coal specimen when it reached the axial compressive strength σ_f . The point of the dissipated energy state $U_{cd}(\varepsilon)$ could be taken as the failure point when it reached the axial compressive strength σ_c . According to the analysis of the relationship between the stress state, damage state and energy state during the failure of the coal specimen, an energy evolution predicting model is constructed based on the dissipated energy state, which can be expressed as Equation (12):

$$\begin{cases} D = 1 - [1 - (\frac{N}{N_f})^{\frac{\beta}{1-\alpha}}] \\ U_d = (1 - \nu) E_0 \frac{1}{1 + e^{-(\varepsilon - \varepsilon_c)^2 + \zeta}} \\ \sigma_c = \frac{1}{\gamma} [\alpha \ln(\frac{\gamma \varepsilon}{\alpha} U_d(\varepsilon) + e^{-\frac{U_0}{\alpha}}) + U_0] \end{cases} \tag{12}$$

Based on the dissipated energy behaviour, the discriminant equation can be used to determine the damage state and stability of the coal specimen. It mainly summarizes the relationship among the dissipative energy state equation, the damage state equation and the strength state equation of the coal specimen.

5. Discussion

5.1. Energy Behaviour Criterion of the Coal Specimen

5.1.1. Energy Storage Factor Criterion

The variation pattern of the dissipative energy storage factor k_{CF} can reflect the energy state and stability of the coal specimen to a large extent. The dissipative energy state has the evolution pattern of "slow growth rate, linear high, rapid growth and slowing rate decrease". Moreover, the dissipative energy storage factor (k_{CF}) also experiences the pattern of "small decline, low value maintenance and then jumping sudden increase". Based on the variation characteristics of the dissipation energy, the dissipative energy storage factor criterion is proposed.

As shown in Figure 13, when $k_{CF} \leq 0.25 \pm 0.03$, the dissipative energy state of the coal specimen is lower, and it is in a stable state. When $0.25 \pm 0.03 \leq k_{CF} \leq 0.5 \pm 0.02$, the dissipative energy state of the coal specimen increases sharply into the critical failure state. When $k_{CF} \geq 0.5 \pm 0.02$, the dissipative energy exceeds the ultimate limitation, and the coal specimen is unstable and broken. It can be indicated that the dissipative energy storage factor criterion can better describe the energy state and stability of the coal specimen in different deformation stages.

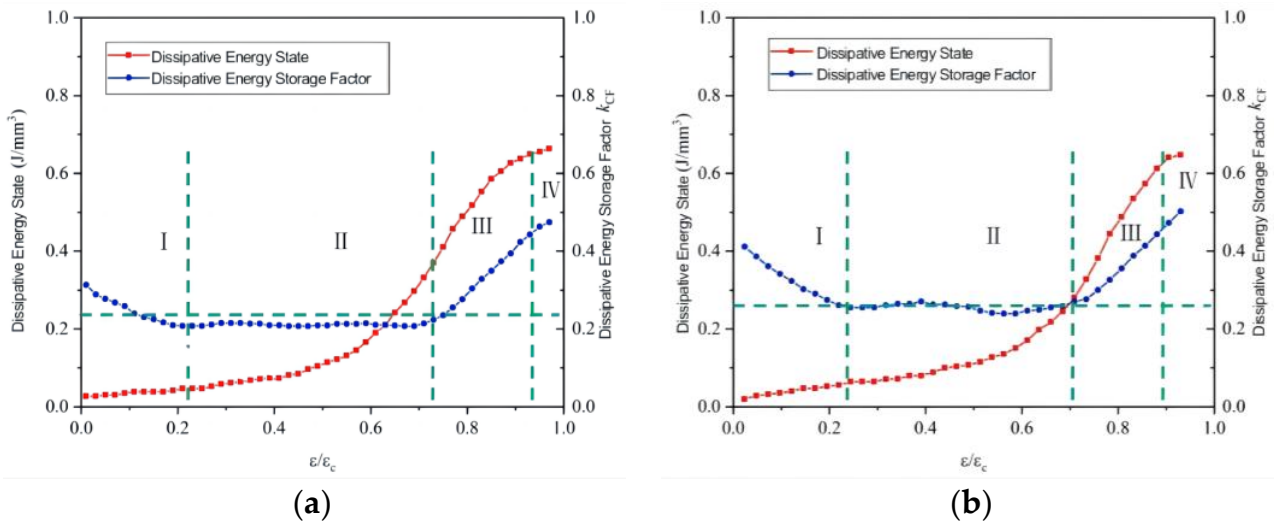


Figure 13. The evolution of energy storage factor during the failure process. The green line is used to delineate the different stages through which the coal samples in the diagram have gone (a) Dissipative energy stage and k_{CF} of the coal sample S1. (b) Dissipative energy stage and k_{CF} of the coal sample S2.

5.1.2. Energy Consumption Growth Factor Criterion

The main reason for coal failure was that the dissipative energy and the elastic strain energy reached a certain equilibrium mechanism. In fact, the elastic strain energy of the coal specimen reached the limitation of its energy storage, and the accumulation of the dissipation energy also reached the maximum state. Therefore, the energy consumption growth factor can better reflect the energy state of the energy storage mechanisms to a large extent. Then, it also can accurately reflect the energy state and stability of the coal specimen. Therefore, the energy consumption growth factor criterion was proposed in this paper.

As shown in Figure 14, when the energy consumption growth factor (k_{HF}) $\leq 0.22 \pm 0.003$, the ratio of the dissipative energy to the elastic energy is at a low value and a small slow decline occurs. The coal specimen is in a stable state at this stage. When $0.22 \pm 0.003 \leq k_{HF} \leq 0.40 \pm 0.002$, the ratio of the dissipative energy to the elastic energy changes to a large extent. The dissipative energy ratio has a sudden growth, and the energy consumption growth factor also has a sudden growth in a short period, the coal specimen is in a critical state of failure. When the energy consumption growth factor $k_{HF} \geq 0.40 \pm 0.002$, the coal specimen has been completely destroyed. It can be known that the energy consumption growth factor criterion of coal specimen can well describe the energy dissipation state and stability state.

5.1.3. Energy Damage Factor Criterion

The generation and variation of the dissipative energy can better reflect the internal fracture and crack of the coal specimen. Therefore, the energy damage factor (k_{DF}) is defined by the dissipative energy, and it is more convincing and accurate to describe the energy state and stability.

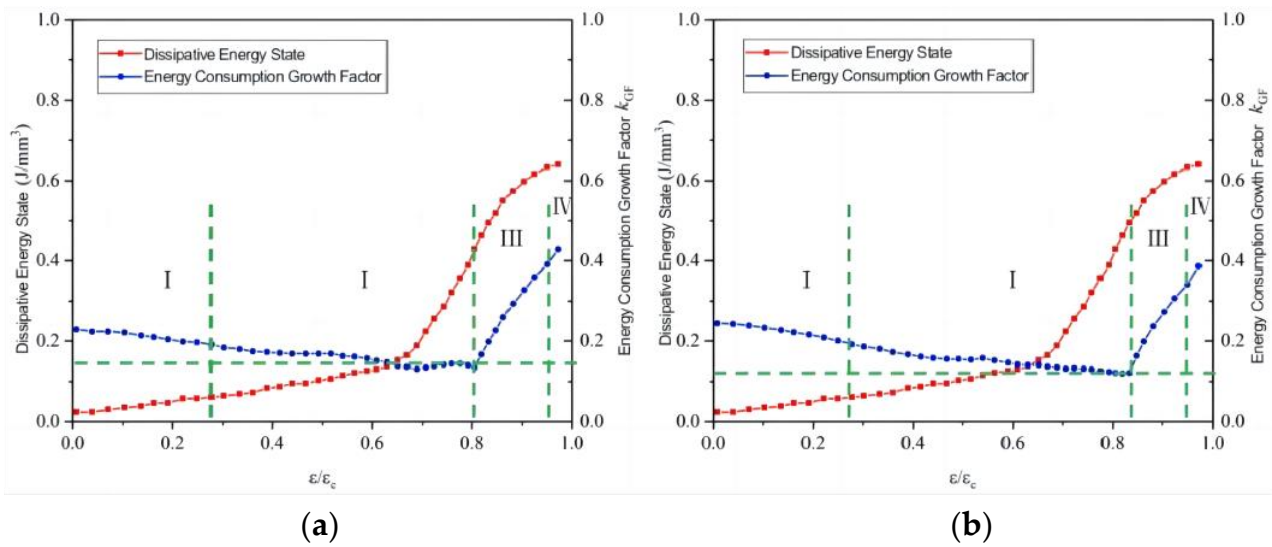


Figure 14. Energy consumption growth factor evolution diagram of coal specimen failure process. The green line is used to delineate the different stages through which the coal samples in the diagram have gone. (a) Dissipative energy stage and k_{CF} of the coal sample S1. (b) Dissipative energy stage and k_{CF} of the coal sample S2.

As shown in Figure 15, when the energy damage factor $k_{DF} \leq 0.32 \pm 0.03$, the damage of the coal specimen is at a lower value. Due to the crack closure and re-cracking, the energy damage factor shows a small rapid rise. When the energy damage factor $0.32 \pm 0.03 \leq k_{DF} \leq 0.50 \pm 0.05$, the damage state of the coal specimen is in a stable and slow linear growth state. When $0.50 \pm 0.05 \leq k_{DF} \leq 1$, the dissipative energy increases suddenly, the stability of the coal specimen also decreases, and it is in a critical stable state. When $k_{DF} = 1$, the coal specimen is in the state of destruction. In fact, it was completely destroyed when the energy damage factor was close to 1 under the axial loading. It can be known that the energy dissipation energy state can distinguish different deformation stages of the coal specimen and it also can better evaluate its stability.

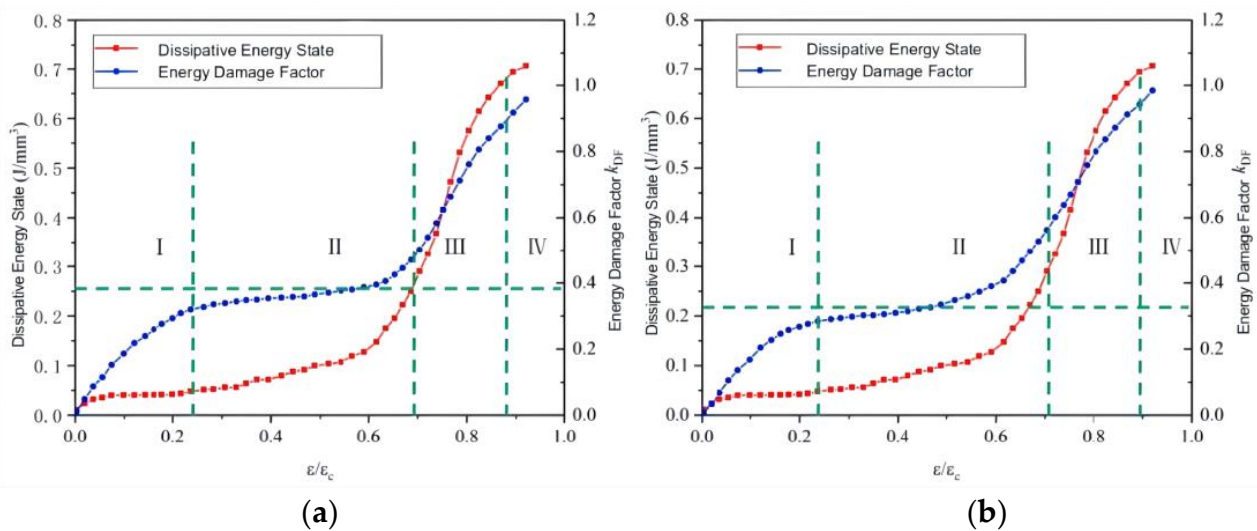


Figure 15. Evolution diagram of energy damage factor in coal specimen failure process. The green line is used to delineate the different stages through which the coal samples in the diagram have gone. (a) Dissipative energy stage and k_{DF} of the coal sample S1. (b) Dissipative energy stage and k_{DF} of the coal sample S2.

5.2. Prototype of Energy Behaviour Predicting Pattern

As shown in Figure 16, it can be known that the criterion of the energy behaviour can better reflect the stable and fracture stage of the coal specimen. Stage I and stage II can be regarded as a stable state in the failure process of the coal specimen. The demarcation point between stage II and stage III can be regarded as the initial predicting point of the coal failure. Furthermore, it is also the turning point of the dissipate energy behaviour of the coal specimen. This point is also the boundary point of the energy state and stability degree of coal specimens.

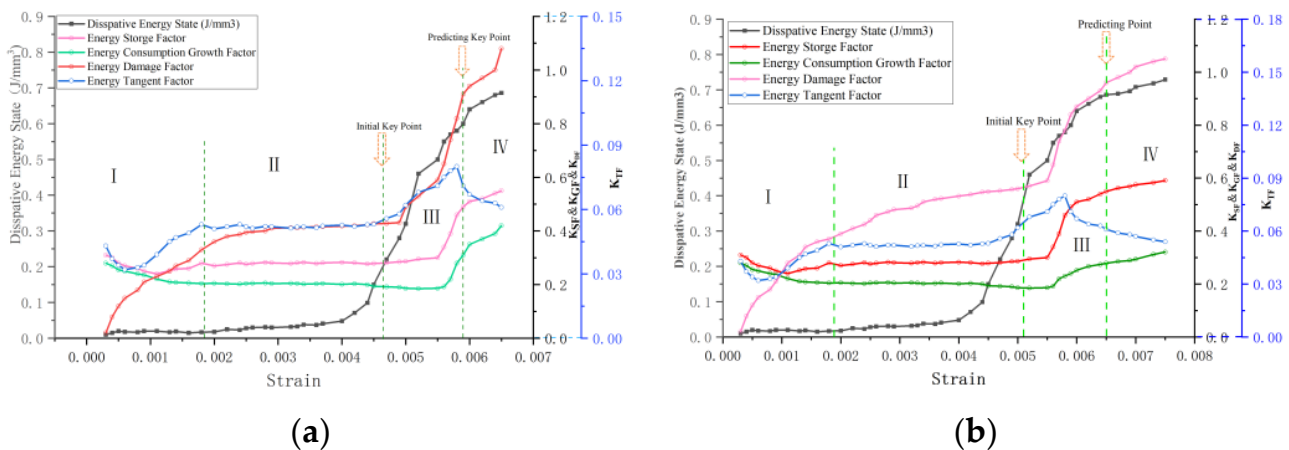


Figure 16. The energy behaviour predicting pattern of the coal failure process. The green line is used to delineate the different stages through which the coal samples in the diagram have gone. (a) Dissipative energy stage, k_{CF} , k_{GF} , k_{DF} and k_{TF} of the coal sample S1. (b) Dissipative energy stage, k_{CF} , k_{GF} , k_{DF} and k_{TF} of the coal sample S2.

The dissipated energy demonstrates a sudden acceleration in stage III. Although coal specimens will not be completely unstable at this stage, it will have produced a large number of cracks and begun to gradually fracture. Then, the dissipation energy of the coal specimen grows faster. The stage IV is regarded as the critical fracture stage of the coal specimen, where the value of the stored dissipation energy is higher, but the growth drops obviously. The internal cracking of the coal specimen has been basically fractured and it is in the critical damage stage.

The demarcation points between stage III and stage IV, namely the peak of the dissipate energy tangent factor, can be regarded as the predicting key point of the coal failure. It is also the inflection point that the growth rate of other energy behaviours slows down. Therefore, it is appropriate to take this point as the key predicting point of coal fracture. Moreover, it can well describe and judge the stable state of the coal specimen. Then, the parameters that are based on the dissipated energy behaviour also show a changing trend of slowing down or decreasing in a relatively short time.

Additionally, many studies were not further enough in this paper, and there are still many problems which need to be further explored in the next studies. The stress gradient was 2 MPa and that is still relatively large. It is difficult to accurately capture the energy behaviour of the coal specimen in the critical failure state. Next, it will be important to continue lowering the gradient to improve the accuracy of the experiment. Ten cycles have been carried out in each stage under the equal amplitude cyclic loading/unloading. This means it is not possible to study the detailed effects of repeated damage on the energy behaviour. Next, the stress gradient will be further reduced, and the number of cycles will be increased to improve the accuracy of the experiment.

6. Conclusions

Based on cyclic loading/unloading experiment and theoretical analysis, the energy behaviour of the coal specimen was analysed. Furthermore, the evolution pattern was also explored in this study. Then, the energy evolution predicting model of the coal specimen was also constructed in this paper, and the following three conclusions were obtained:

- (1) The energy density of the coal specimen has experienced the evolution pattern of “slow growth rate–linear high speed growth–slowing growth rate” under the staged cycle loading/unloading. Furthermore, the energy storage state of the coal specimen has experienced “lower value–extreme speed growth–stable value–a small decline”. Under the equal amplitude loading/unloading, the energy density gradually decreases in stage I and stage III. It basically maintains a stable state without a large degree of fluctuation in stage II, and its energy storage rate has undergone the evolution pattern of “high value–higher value–medium-to-high value”.
- (2) The coal specimen exhibits different energy behaviours and energy states in different fracture stages. The energy behaviours of the coal specimen can well reflect the steady state of different deformation stages of the coal failure, and the dissipative energy behaviour has a sudden effect in the fracture process. This contributes to describing the sudden characteristics of the coal failure. The energy-driven mechanism of coal failure is determined by the energy storage mechanism and the energy consumption mechanism. It is related to the energy storage limit and the energy consumption limit. The energy storage mechanism of the coal specimen presents the pattern of “low energy promotion, high energy suppression and dissipation promotion, cumulative suppression growth”.
- (3) Based on the energy dissipation behaviour of the coal specimen, the damage state evolution equation and the energy behaviour evolution criterion are established under the cyclic loading/unloading. Then, an energy evolution predicting model of the coal specimen is constructed in this paper.

Author Contributions: Conceptualization, C.W. and Z.Z.; methodology, C.W.; data curation, Z.Z. and C.Z.; writing—review and editing, C.W., Z.Z. and C.Z.; writing—original draft, Z.Z.; funding acquisition, C.W. All authors have read and agreed to the published version of the manuscript.

Funding: This research was funded by the National Natural Science Foundation of China (Grant No. 52074294) and the Fundamental Research Funds for the Central Universities (Grant No. 2022YJSNY16).

Institutional Review Board Statement: Not applicable.

Informed Consent Statement: Not applicable.

Data Availability Statement: All data, models or code that support the findings of this study are available from the corresponding author upon reasonable request.

Acknowledgments: We thank the anonymous reviewers for their support to this study.

Conflicts of Interest: The authors declare no conflict of interest.

References

1. Eberhardt, E.; Stead, D.; Stimpson, B. Identifying crack initiation and propagation thresholds in brittle rock. *Can. Geotech. J.* **1998**, *35*, 222–233. [\[CrossRef\]](#)
2. Cai, M.; Kaiser, P.K.; Tasaka, Y. Generalized crack initiation and crack damage stress thresholds of brittle rock masses near underground excavations. *Int. J. Rock Mech. Min.* **2004**, *41*, 833–847. [\[CrossRef\]](#)
3. Wang, C.L.; Gao, A.S.; Shi, F. Three-dimensional Reconstruction and Growth Factor Model for Rock Cracks under Uniaxial Cyclic Loading/Unloading by X-ray CT. *Geotech. Test. J.* **2019**, *42*, 117–135. [\[CrossRef\]](#)
4. Vejahati, F.; Xu, Z.H.; Gupta, R. Trace elements in coal: Associations with coal and minerals and their behavior during coal utilization—A review. *Fuel* **2010**, *89*, 904–911. [\[CrossRef\]](#)
5. Deng, Y.; Chen, M.; Jin, Y. Theoretical analysis and experimental research on the energy dissipation of rock crushing based on fractal theory. *J. Nat. Gas. Sci. Eng.* **2016**, *33*, 231–239. [\[CrossRef\]](#)

6. Munoz, H.; Taheri, A.; Chanda, E.K. Fracture energy-based brittleness index development and brittleness quantification by pre-peak strength parameters in rock uniaxial compression. *Rock Mech. Rock Eng.* **2016**, *49*, 4587–4606. [[CrossRef](#)]
7. Li, X.L.; Chen, S.J.; Li, Z.H. Rockburst mechanism in coal rock with structural surface and the microseismic (MS) and electromagnetic radiation (EMR) response. *Eng. Fail. Anal.* **2021**, *124*, 105396. [[CrossRef](#)]
8. Wang, C.L.; Liu, Y.B.; Hou, X.L.; Elmo, D. Investigation of the spatial distribution pattern of 3D microcracks in single-cracked breakage. *Int. J. Rock Mech. Min. Sci.* **2022**, *154*, 105126. [[CrossRef](#)]
9. Wang, C.L.; Zhou, B.K.; Li, C.F. Experimental investigation on the spatio-temporal-energy evolution pattern of limestone fracture using acoustic emission monitoring. *J. Appl. Geophys.* **2022**, *206*, 104787. [[CrossRef](#)]
10. Wang, C.L.; Hou, X.L.; Liu, Y.B. Three-Dimensional Crack Recognition by Unsupervised Machine Learning. *Rock Mech. Rock Eng.* **2021**, *54*, 893–903. [[CrossRef](#)]
11. Li, X.L.; Chen, S.J.; Liu, S.M. AE waveform characteristics of rock mass under uniaxial loading based on Hilbert-Huang transform. *J. Cent. South Univ.* **2021**, *28*, 1843–1856. [[CrossRef](#)]
12. Cerfontaine, B.; Collin, F. Cyclic and fatigue behaviour of rock materials: Review, interpretation and research perspectives. *Rock Mech. Rock Eng.* **2018**, *51*, 391–414. [[CrossRef](#)]
13. Taheri, A.; Yfantidis, N.; Olivares, C.L. Experimental study on degradation of mechanical properties of sandstone under different cyclic loadings. *Geotech. Test. J.* **2016**, *39*, 673–687. [[CrossRef](#)]
14. Feng, F.; Chen, S.J.; Wang, Y.J. Cracking mechanism and strength criteria evaluation of granite affected by intermediate principal stresses subjected to unloading stress state. *Int. J. Rock Mech. Min.* **2021**, *143*, 104783. [[CrossRef](#)]
15. Zhang, M.; Meng, Q.; Liu, S. Energy evolution characteristics and distribution laws of rock materials under triaxial cyclic loading and unloading compression. *Adv. Mater. Sci. Eng.* **2017**, *8*, 5471571. [[CrossRef](#)]
16. Wang, C.L.; Hou, X.L.; Liao, Z.F. Experimental investigation of predicting coal failure using acoustic emission energy and load-unload response ratio theory. *J. Appl. Geophys.* **2019**, *161*, 76–83. [[CrossRef](#)]
17. Gong, F.; Luo, S.; Yan, J. Energy storage and dissipation evolution process and characteristics of marble in three tension-type failure tests. *Rock Mech. Rock Eng.* **2018**, *51*, 3613–3624. [[CrossRef](#)]
18. Hua, A.Z.; You, M.Q. Rock failure due to energy release during unloading and application to underground rock burst control. *Tunn. Undergr. Sp. Technol.* **2001**, *3*, 241–246. [[CrossRef](#)]
19. Xiao, J.Q.; Ding, D.X.; Jiang, F.L. Fatigue damage variable and evolution of rock subjected to cyclic loading. *Int. J. Rock Mech. Min.* **2010**, *3*, 461–468. [[CrossRef](#)]
20. Liu, E.; He, S. Effects of cyclic dynamic loading on the mechanical properties of intact rock samples under confining pressure conditions. *Eng. Geol.* **2012**, *125*, 81–91. [[CrossRef](#)]
21. Wang, Y.; Cui, F. Energy evolution mechanism in process of Sandstone failure and energy strength criterion. *J. Appl. Geophys.* **2018**, *154*, 21–28. [[CrossRef](#)]
22. Chen, Z.; He, C.; Ma, G. Energy Damage Evolution Mechanism of Rock and Its Application to Brittleness Evaluation. *Rock Mech. Rock Eng.* **2019**, *52*, 1265–1274. [[CrossRef](#)]
23. He, M.; Huang, B.; Zhu, C. Energy dissipation-based method for fatigue life prediction of rock salt. *Rock Mech. Rock Eng.* **2018**, *51*, 1447–1455. [[CrossRef](#)]
24. Bagde, M.N.; Petroš, V. Fatigue properties of intact sandstone samples subjected to dynamic uniaxial cyclical loading. *Int. J. Rock Mech. Min.* **2005**, *42*, 237–250. [[CrossRef](#)]
25. Bagde, M.N.; Petroš, V. Fatigue and dynamic energy behaviour of rock subjected to cyclical loading. *Int. J. Rock Mech. Min.* **2009**, *46*, 200–207. [[CrossRef](#)]
26. Sun, B.; Zhu, Z.; Shi, C. Dynamic mechanical behaviour and fatigue damage evolution of sandstone under cyclic loading. *Int. J. Rock Mech. Min.* **2017**, *94*, 82–89. [[CrossRef](#)]
27. Huang, D.; Li, Y. Conversion of strain energy in triaxial unloading tests on marble. *Int. J. Rock Mech. Min.* **2014**, *66*, 160–168. [[CrossRef](#)]
28. Li, D.; Sun, Z.; Xie, T. Energy evolution characteristics of hard rock during triaxial failure with different loading and unloading paths. *Eng. Geol.* **2017**, *228*, 270–281. [[CrossRef](#)]
29. Jiang, C.; Duan, M.; Yin, G. Experimental study on seepage properties, AE characteristics and energy dissipation of coal under tiered cyclic loading. *Eng. Geol.* **2017**, *221*, 114–123. [[CrossRef](#)]
30. Ning, J.; Wang, J.; Jiang, J. Estimation of crack initiation and propagation thresholds of confined brittle coal specimens based on energy dissipation theory. *Rock Mech. Rock Eng.* **2018**, *51*, 119–134. [[CrossRef](#)]
31. Yang, Y.; Duan, H.Q.; Xing, L.Y.; Deng, L. Fatigue Characteristics of Coal Specimens under Cyclic Uniaxial Loading. *Geotech. Test. J.* **2019**, *42*, 331–346. [[CrossRef](#)]
32. Wang, Z.; Li, H.R.; Wang, J.G.; Shi, H. Experimental Study on Mechanical and Energy Properties of Granite under Dynamic Triaxial Condition. *Geotech. Test. J.* **2018**, *41*, 1063–1075. [[CrossRef](#)]
33. Meng, Q.; Zhang, M.; Han, L. Effects of acoustic emission and energy evolution of rock specimens under the uniaxial cyclic loading and unloading compression. *Rock Mech. Rock Eng.* **2016**, *49*, 3873–3886. [[CrossRef](#)]
34. Peng, R.; Ju, Y.; Wang, J.G. Energy dissipation and release during coal failure under conventional triaxial compression. *Rock Mech. Rock Eng.* **2015**, *48*, 509–526. [[CrossRef](#)]

35. Vaneghi, R.G.; Ferdosi, B.; Okoth, A.D.; Kuek, B. Strength degradation of sandstone and granodiorite under uniaxial cyclic loading. *J. Rock Mech. Geotech. Eng.* **2018**, *10*, 117–126. [[CrossRef](#)]
36. Chen, W.X.; He, X.Q.; Liu, M.J.; Mitri, H.; Wang, Q. Meso- and macro-behaviour of coal rock: Observations and constitutive model development. *Int. J. Rock Mech. Min.* **2015**, *30*, 13–24. [[CrossRef](#)]
37. Xu, J.; Jiang, J.; Xu, N. A new energy index for evaluating the tendency of rockburst and its engineering application. *Eng. Geol.* **2017**, *230*, 46–54. [[CrossRef](#)]
38. Liu, X.S.; Ning, J.G.; Tan, Y.L. Damage constitutive model based on energy dissipation for intact rock subjected to cyclic loading. *Int. J. Rock Mech. Min.* **2016**, *85*, 27–32. [[CrossRef](#)]
39. Meng, Q.; Zhang, M.W.; Zhang, Z.Z. Experimental Research on Rock Energy Evolution under Uniaxial Cyclic Loading and Unloading Compression. *Geotech. Test. J.* **2018**, *41*, 717–729. [[CrossRef](#)]
40. Wang, C.L. *Evolution, Monitoring and Predicting Models of Rockburst*; Springer: Berlin/Heidelberg, Germany, 2018. [[CrossRef](#)]
41. Munoz, H.; Taheri, A.; Chanda, E.K. Rock drilling performance evaluation by an energy dissipation based rock brittleness index. *Rock Mech. Rock Eng.* **2016**, *49*, 3343–3355. [[CrossRef](#)]
42. Wang, C.L.; He, B.B.; Hou, X.L. Stress-Energy Mechanism for Rock Failure Evolution Based on Damage Mechanics in Hard Rock. *Rock Mech. Rock Eng.* **2019**, *53*, 1021–1037. [[CrossRef](#)]
43. Hoek, E.; Martin, C.D. Fracture initiation and propagation in intact rock—A review. *J. Rock Mech. Geotech. Eng.* **2014**, *6*, 287–300. [[CrossRef](#)]
44. Munoz, H.; Taheri, A. Local Damage and Progressive Localisation in Porous Sandstone during Cyclic Loading. *Rock Mech. Rock Eng.* **2017**, *50*, 3253–3259. [[CrossRef](#)]
45. Munoz, H.; Taheri, A.; Chanda, E. Rock cutting characteristics on soft-to-hard rocks under different cutter inclinations. *Int. J. Rock Mech. Min.* **2016**, *87*, 85–89. [[CrossRef](#)]
46. Zhao, G.; Bing, D.A.I.; Dong, L. Energy conversion of rocks in process of unloading confining pressure under different unloading paths. *Trans. Nonferrous Met. Soc. China* **2015**, *25*, 1626–1632. [[CrossRef](#)]
47. Xie, H.; Li, L.; Peng, R. Energy analysis and criteria for structural failure of rocks. *J. Rock Mech. Geotech. Eng.* **2009**, *1*, 11–20. [[CrossRef](#)]
48. Wang, Q.S.; Chen, J.X.; Guo, J.Q.; Luo, Y.B.; Wang, H.Y.; Liu, Q. Acoustic emission characteristics and energy mechanism in karst limestone failure under uniaxial and triaxial compression. *Bull. Eng. Geol. Environ.* **2019**, *78*, 1427–1442. [[CrossRef](#)]
49. Tarasov, B.G.; Stacey, T.R. Features of the Energy Balance and Fragmentation Mechanisms at Spontaneous Failure of Class I and Class II Rocks. *Rock Mech. Rock Eng.* **2017**, *50*, 2563–2584. [[CrossRef](#)]

Disclaimer/Publisher’s Note: The statements, opinions and data contained in all publications are solely those of the individual author(s) and contributor(s) and not of MDPI and/or the editor(s). MDPI and/or the editor(s) disclaim responsibility for any injury to people or property resulting from any ideas, methods, instructions or products referred to in the content.